# Monitoring seismic velocity change caused by the 2011 Tohoku-oki earthquake using ambient noise records

Shohei Minato,[1] Takeshi Tsuji,[2] Shiro Ohmi,[3] and Toshifumi Matsuoka[1]

Received 19 February 2012; revised 6 April 2012; accepted 9 April 2012; published 12 May 2012.

[1] We estimated the changes in seismic velocity in the southern Tohoku district of Japan during the six-month period centered on the 11 March 2011 Tohoku-oki earthquake, using scattered waves retrieved by autocorrelation of ambient seismic noise. The estimated velocity decrease after the earthquake, and after two large aftershocks in the study area, was as great as 1.5% in the area nearest to the mainshock. The velocity changes displayed gradual healing. The spatial distribution of the velocity change showed a correlation with both the changes in static strain, derived from GPS records, and the peak particle velocity experienced during the three earthquakes, derived from strong-motion records. Therefore, our results show that velocity changes possibly contain information from deep in the crust bearing on coseismic stress release, in addition to shallower effects due to strong ground motion. **Citation:** Minato, S., T. Tsuji, S. Ohmi, and T. Matsuoka (2012), Monitoring seismic velocity change caused by the 2011 Tohoku-oki earthquake using ambient noise records, *Geophys. Res. Lett.*, *39*, L09309, doi:10.1029/2012GL051405.

## 1. Introduction

[2] Seismic interferometry, or reverse-time acoustics, is used to retrieve the impulse response from cross-correlation of the wavefield [e.g., *Derode et al.*, 2003; *Roux et al.*, 2005; *Wapenaar and Fokkema*, 2006; *Larose et al.*, 2006]. The continuously observed wavefield of ambient seismic noise can be used, in the method called passive image interferometry, to monitor the dynamic change of the medium. Applications of seismic interferometry to ambient noise have been used to retrieve surface waves and estimate their group velocity distribution [*Shapiro et al.*, 2005] and to retrieve the reflection response [*Draganov et al.*, 2009]. The retrieval of scattered waves is alternatively used to detect small changes in the propagating velocity [*Sens-Schönfelder and Wegler*, 2006; *Brenguier et al.*, 2008; *Meier et al.*, 2010]. The autocorrelation of the ambient noise is interpreted as the source-receiver colocated (zero-offset) seismic response. *Wegler and Sens-Schönfelder* [2007] and *Ohmi et al.* [2008] have used the autocorrelation function (ACF) to monitor the temporal change of the impulse response triggered by earthquakes.

[3] Earthquakes are known to cause seismic velocity changes in crustal rocks by several mechanisms. Research has long shown that velocity shows dependency on static stress conditions [e.g., *Toksöz et al.*, 1976; *Christensen and Wang*, 1985; *Tsuji et al.*, 2008]. Several studies have observed the velocity change associated with stress change due to earthquakes by using multiplet earthquake analysis [e.g., *Poupinet et al.*, 1984] or controlled source experiments [e.g., *Nishimura et al.*, 2000; *Niu et al.*, 2008]. Another cause of velocity change is nonlinear fast dynamics (NFD) and slow dynamics (SD), in which the elastic properties evolve in response to stress-strain conditions beyond the assumption of linear elasticity [e.g., *Lyakhovsky et al.*, 1997; *TenCate et al.*, 2000; *Johnson and Sutin*, 2005]. Recent studies have documented velocity change associated with effects of strong ground motion by using multiplet earthquakes [*Schaff and Beroza*, 2004; *Rubinstein and Beroza*, 2004; *Peng and Ben-Zion*, 2006] and controlled source experiments [*Vidale and Li*, 2003]. A few studies using passive image interferometry have detected velocity changes that possibly reflect the effects of stress change and/or near-surface damage due to strong shaking [e.g., *Wegler and Sens-Schönfelder*, 2007; *Brenguier et al.*, 2008; *Wegler et al.*, 2009].

[4] GPS network observations of the giant Tohoku-oki earthquake of 11 March 2011 (Mw 9.0) revealed that the coseismic displacement included eastward movement of up to 5.3 m and subsidence of up to 1.2 m in the eastern Japanese island arc [*Ozawa et al.*, 2011]. This large displacement caused enormous strain change in the Tohoku region [*Takahashi*, 2011; *Yoshida et al.*, 2012]. The earthquake also caused widespread strong ground motion. Therefore, we sought to monitor velocity changes in the southern Tohoku region and assess their causes using ambient seismic records from the Japanese Hi-net system.

## 2. Method

[5] Autocorrelation of ambient noise records yields the seismic response for a coincident source and receiver position [e.g., *Wapenaar and Fokkema*, 2006]. The method assumes that the noise source is mutually uncorrelated for different source positions [e.g., *Weaver and Lobkis*, 2004; *Roux et al.*, 2005; *Wapenaar and Fokkema*, 2006]; therefore, the phase of the noise source should be random, and earthquakes, with their deterministic phases, are regarded as anomalies. We applied running absolute amplitude normalization [*Bensen et al.*, 2007] to suppress earthquakes. The window size used for the normalization affects the weighting range to suppress strong amplitudes. We found that the size of the window significantly affected the traveltime of coherent events in the ACF, and after careful investigation we selected a window length of 25 s. We also applied zero-phase amplitude whitening to balance the frequency

[1]Graduate School of Engineering, Kyoto University, Kyoto, Japan.
[2]Now at International Institute for Carbon-Neutral Energy Research (I2CNER), Kyushu University, Fukuoka, Japan.
[3]Disaster Prevention Research Institute, Kyoto University, Kyoto, Japan.

Corresponding author: S. Minato, International Institute for Carbon-Neutral Energy Research (I2CNER), Kyushu University, Fukuoka, Japan. (s_minato@earth.kumst.kyoto-u.ac.jp)


0094-8276/12/2012GL051405

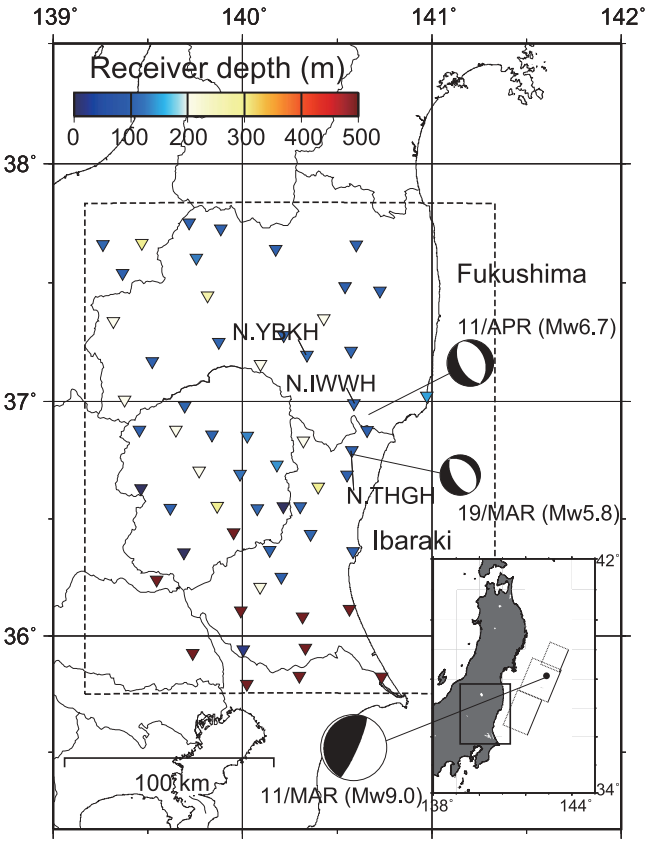


**Figure 1.** Survey area map showing positions and depths of 58 Hi-net stations (triangles). A color of station shows the station depth. The color of station deeper than 500 m is fixed. Locations and focal mechanisms are shown for the Tohoku-oki earthquake mainshock (Mw 9.0, 11 March, in inset), North Ibaraki aftershock (Mw 5.8, 19 March), and South Fukushima aftershock (Mw 6.7, 11 April). Fault model of mainshock is from *Nishimura et al.* [2011]. Three individual stations (N.YBKH, N.IWWH, and N.THGH) are labeled.

component [*Bensen et al.*, 2007; *Meier et al.*, 2010]. We used a moving average of the amplitude and a damping factor of 5% of the maximum amplitude to stabilize the whitening.

[6] To estimate the velocity perturbation due to earthquakes, we applied the stretching interpolation technique [e.g., *Sens-Schönfelder and Wegler*, 2006; *Hadziioannou et al.*, 2009]. The resulting ACF represents the zero-offset seismic response and contains the scattered wave with the traveltime perturbation evolving each day. The method elongates the time axis, interpolates the amplitudes of the calculated trace, and searches for the parameter value that produces a waveform most similar to the reference trace:

$$f_{\epsilon}^{cur}(t) = f^{cur}(t(1+\epsilon)), \tag{1}$$

$$C(\epsilon) = \frac{\int f_{\epsilon}^{cur}(t) f^{ref}(t)dt}{\left(\int \left(f_{\epsilon}^{cur}(t)\right)^2 dt \int \left(f^{ref}(t)\right)^2 dt\right)^{\frac{1}{2}}}, \tag{2}$$

where $\epsilon$ is a stretching parameter, $f^{ref}$ represents the reference trace, $f^{cur}$ represents the current trace, and $C(\epsilon)$ is the correlation coefficient between the reference and elongated traces. We searched for the value of $\epsilon$ yielding the maximum value of $C$ in equation (2) by adopting a grid search algorithm. Since a part of data showed multiple local maxima, we manually picked the local maxima that yielded the smoothest transitions from day to day. The stretch parameter $\epsilon$ corresponds to a relative time-shift ($\Delta t/t$) of the dominant event, and we assumed that it relates to a relative velocity change ($\Delta v/v$) as [*Hadziioannou et al.*, 2009],

$$\epsilon = \frac{\Delta t}{t} = -\frac{\Delta v}{v}. \tag{3}$$

[7] Note that in this analysis we assume that (1) the autocorrelated trace is dominated by the scattered wave generated from the subsurface and (2) the traveltime perturbation directly corresponds to the velocity perturbation, which indicates that the velocity perturbation is homogeneous in the medium, or at least in the region where the scattered waves propagate within the specified time window.

## 3. Data and Result

### 3.1. Survey Area

[8] The survey area includes Fukushima and Ibaraki prefectures in the southern Tohoku district (Figure 1). Although the maximum depth of the Hi-net stations is 3500 m, most stations are 100 m to 200 m deep (Figure 1). We used the vertical component of the records from 58 Hi-net stations from 9 January to 30 June 2011, a total of 173 days. During that time, the survey area experienced at least two aftershocks causing a large surface deformation that was detected in satellite observations (interferometric synthetic aperture radar or InSAR) of the Geospatial Information Authority of Japan (GSI). These were the North Ibaraki event of 19 March (Mw 5.8, 10 km deep) and the South Fukushima event of 11 April (Mw 6.7, 10 km deep) (Figure 1). The fault traces on the ground estimated from InSAR are approximately 7 km in the North Ibaraki event and 14 km in the South Fukushima event (Geospatial Information Authority of Japan (GSI), 2011, http://www.gsi.go.jp).

### 3.2. ACF and Temporal Variation of the Velocity Perturbation

[9] We autocorrelated each day of seismic data and obtained 173 ACFs for each of the 58 Hi-net stations. A typical ACF record is that of station N.YBKH (Figure 2a), which shows data for the 2–10 s traveltime interval after bandpass filtering between 2 and 5 Hz. Data for the period 13–14 March were not available. A coherent event is apparent in the ACF, and its characteristics changed after 11 March. We show the temporal change in the velocity (traveltime) perturbation ($\epsilon$) at station N.YBKH in Figure 2b for the 2–10 s period. We stacked all ACFs to obtain the reference trace for equation (2) and as a calculated trace we used each 1-day ACF after the application of a 5-day moving average window. We calculated $C(\epsilon)$ for a range of $-10\% \leq \epsilon \leq 10\%$ with $\Delta\epsilon = 0.1\%$ and picked maximum values after spline interpolation. Because the averaged waveform was defined as the zero percentage perturbation, $\epsilon$ starts from around $-0.5\%$. A positive value of $\epsilon$ indicates that traveltime was longer (velocity was slower) in the current trace than in the reference trace. The sudden change of $\epsilon$ on 11 March corresponds to the Tohoku-oki mainshock, when the velocity

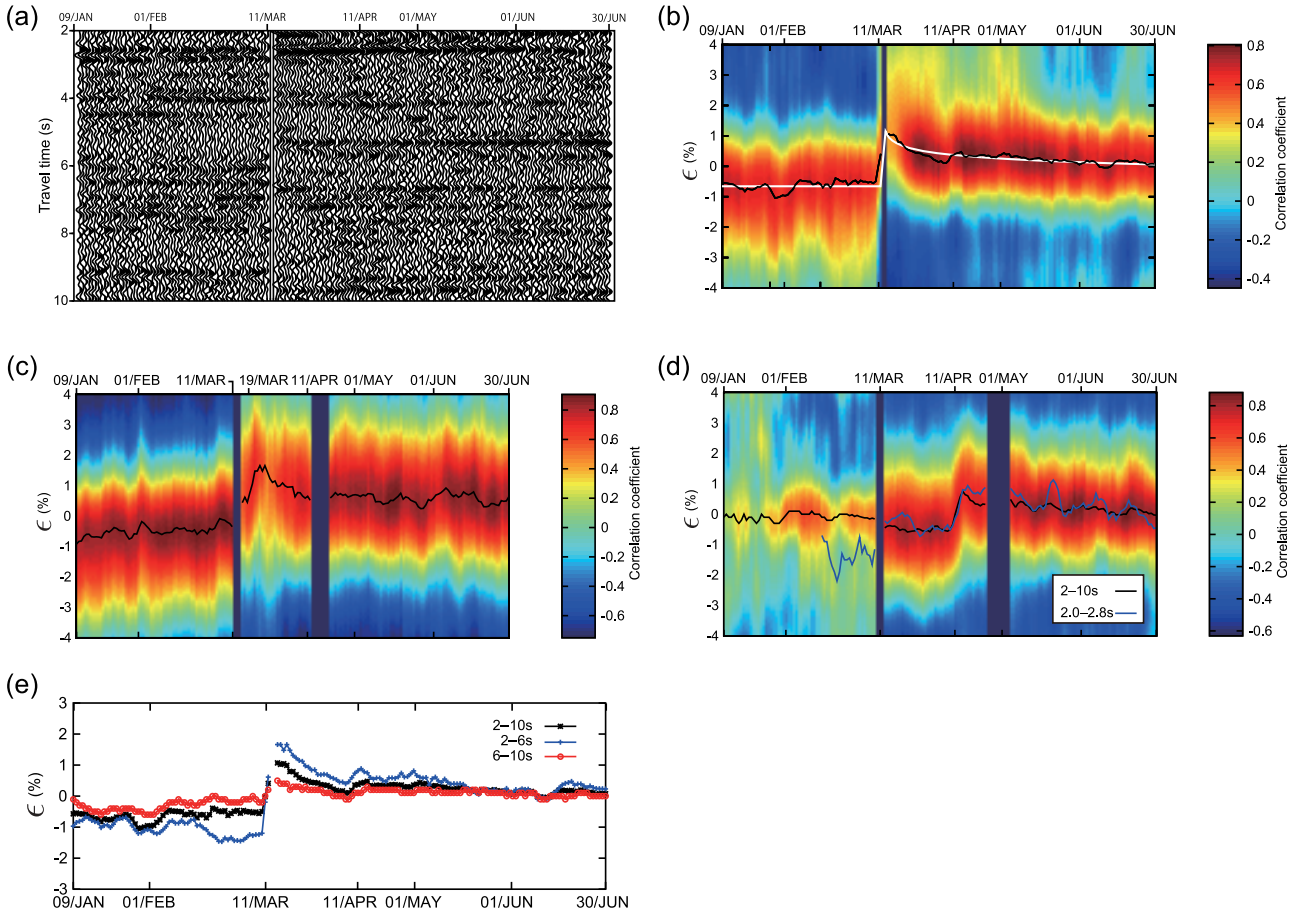


**Figure 2.** (a) Autocorrelation function at station N.YBKH after bandpass filtering for 2–5 Hz. Temporal variation of the velocity change ($\epsilon$) and the correlation coefficient of stretching interpolation technique at stations (b) N.YBKH, (c) N.THGH, and (d) N.IWWH. White line in Figure 2b indicates the fitted logarithmic curve. Blue line in Figure 2d indicates the estimated $\epsilon$ with the lag times of 2.0 s – 2.8 s. There are several data gaps around 11 March for Figures 2b–2d, 13 April for Figure 2c and 1 May for Figure 2d. (e) Calculated velocity change at station N.YBKH for different lag times. Station locations in Figure 1.

dropped 2%. A gradual recovery of the velocity [e.g., *Peng and Ben-Zion*, 2006; *Vidale and Li*, 2003; *Schaff and Beroza*, 2004; *Rubinstein and Beroza*, 2004] was observed after the Tohoku-oki earthquake. This observation matches that of another study focusing on near-surface velocity change due to the Tohoku-oki earthquake [*Nakata and Snieder*, 2011]. We fit this healing curve with the logarithmic line $\epsilon(d) = a\log_{10}(d) + b$, where $d$ is the elapsed day, $b$ corresponds to the maximum $\epsilon$ and obtained the coefficient ($a$) as $-0.53$ (white line in Figure 2b). This relation indicates that the velocity recovered to 99% of its preseismic value a month after the mainshock. This time-scale of the recovery is consistent with a decrease of the shear modulus due to strong ground motion, as suggested by *Sawazaki et al.* [2009]. The coseismic velocity perturbation remained around 0.5% 100 days after the earthquake.

[10] Station N.THGH (Figure 2c) is near the fault that ruptured in the North Ibaraki aftershock of 19 March (Figure 1). It is apparent that the maximum change in velocity was later than in Figure 2b and that the velocity changed in two steps, caused by two earthquakes: the 11 March event caused a 0.8% perturbation and the 19 March event caused a further 1% perturbation.

[11] Station N.IWWH (Figure 2d) is near the fault that ruptured in the South Fukushima aftershock of 11 April (Figure 1). As the waveforms before and after 11 March are very different, the correlation coefficient in the stretch analysis has low values in the pre-mainshock period (Figure 2d). Furthermore the velocity perturbation did not show a discontinuity on 11 March (black line in Figure 2d). This lack of discontinuity might be due to the effects of strong near-surface deformation, the change in seismicity that was not fully removed before autocorrelation, or the change in the source characteristics of the ambient noise. We focused on the dominant events appearing at 2.0–2.8 s and calculated $\epsilon$ using that small time window (blue line in Figure 2d). We could track these events from 20 February to 30 June. The resulting curve shows less stability than the curve generated with the longer time window; however, it shows a strong velocity drop on 11 March and closely tracks the other curve in the post-earthquake period (Figure 2d). The results clearly show velocity reductions caused by the two earthquakes of 11 March and 11 April.

[12] The stretching interpolation technique (equations (1) and (2)) assumes a homogeneous velocity change within the time window. However, the scattering events at different traveltimes (lag times in ACF) may propagate through different regions of the subsurface, and consequently they may contain information about different depths. Therefore, we investigated the use of equations (1) and (2) with different lag

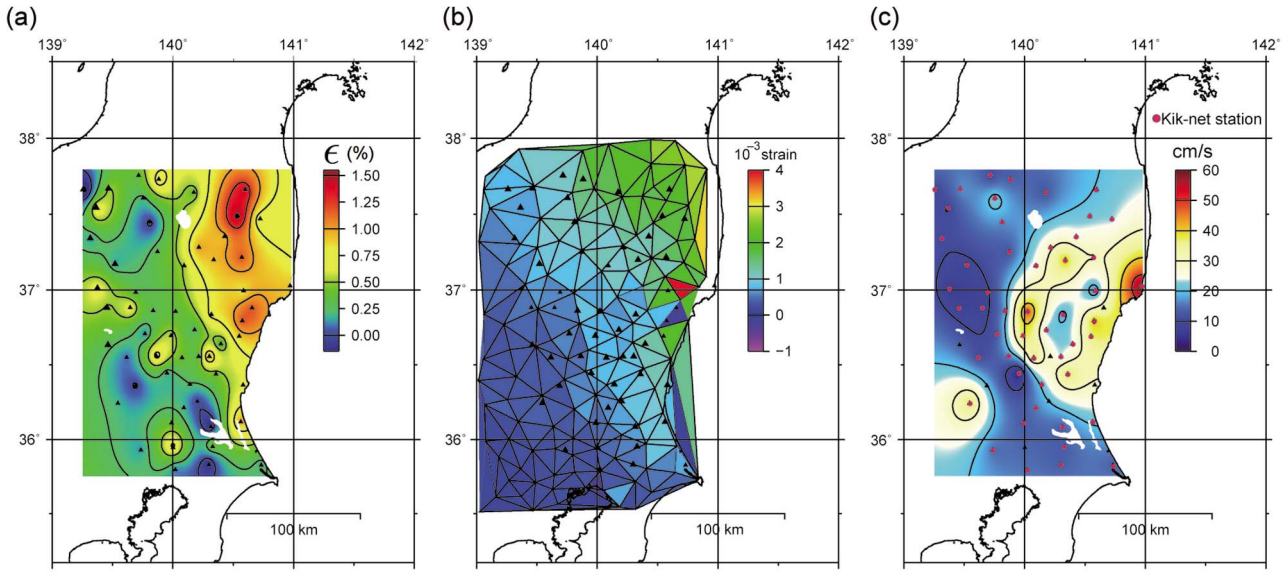


**Figure 3.** (a) Averaged spatial distribution of velocity change between preseismic (9 January to 10 March) and postseismic (11 March to 30 June) period. (b) Static area strain change derived from GPS records at stations located at each triangle apex. Strain is calculated from the change in coordinates between 1 January and 29 June 2011. (c) Spatial distribution of the cumulative peak particle velocities recorded in three earthquakes (11 March, 19 March, and 11 April) by Kik-net stations colocated with Hi-net stations.

times. Figure 2e shows the calculated velocity perturbations at station N.YBKH for lag times of 2–10 s, 2–6 s, and 6–10 s. The coseismic jump at 11 March with the lag time of 2–6 s (approximately 3%) is larger than that with the lag time of 6–10 s (approximately 0.5%). This may indicate that coherent events with longer traveltime propagate through deeper structures, and the shallower subsurface experienced larger velocity reductions than the deeper subsurface. The result with the lag time of 2–10 s represents an average of values in the other two lag times.

### 3.3. Spatial Variation of the Velocity Change

[13] Observations at some stations were interrupted by strong shaking and the velocity perturbation gradually healed, as shown in Figure 2b. In analyzing the spatial distribution of the velocity change, we therefore attempted to minimize these factors by calculating the difference between the averaged velocity change between the preseismic (9 January-10 March) and postseismic (11 March-30 June) periods (Figure 3a).

[14] Figure 3a, produced using a kriging interpolation, shows that the eastern part of the study area near the coast had larger velocity reductions than the western part. The maximum velocity change was approximately 1.5% in the eastern area. Nearly the entire region showed a velocity decrease; we believe that the small velocity increases in a few places are within the uncertainties of our method.

## 4. Discussion and Conclusion

[15] We detected notable velocity changes during the six-month period encompassing the Tohoku-oki earthquake using scattered waves retrieved by autocorrelation of ambient noise. In this section we evaluate two likely reasons for these velocity changes. First, earthquakes produce changes in the regional stress field, and rock physics modeling predicts velocity changes arising from the change in effective pressure due to the opening or closing of cracks [e.g., *Toksöz et al.*, 1976]. Second, coseismic strong motions may cause nonlinear behavior of elastic properties of the lithosphere [e.g., *Vidale and Li*, 2003; *Schaff and Beroza*, 2004; *Peng and Ben-Zion*, 2006]. In this study, we try to use a static strain change and a peak particle velocity as the indicators of stress change and strong motions respectively because these can be estimated from observable quantities in the field.

[16] Static strain change can be derived from GPS records from the GEONET network operated by the GSI. We used horizontal displacements from GPS GEONET F3 daily coordinate records over the survey period to calculate static area strain (summation of normal strain for two horizontal axes) change, derived by using the constant strain triangle element method [e.g., *Terada and Miyabe*, 1929]. Figure 3b shows the estimated static area strain change between 1 January and 29 June 2011. The Tohoku-oki earthquake caused almost the whole survey region to experience dilatation (positive area strain change). The largest amounts of dilatation were near the coastline, corresponding to the large velocity change we estimated by passive image interferometry (Figure 3a). The polygon of unusually large dilatation in Figure 3b is a consequence of the two aftershocks at North Ibaraki (19 March) and South Fukushima (11 April).

[17] We also compared the estimated velocity changes to the spatial distribution of peak particle velocity from the Kik-net strong-motion network, during the three earthquakes in the study period (Figure 3c). Kik-net stations are collocated with almost all Hi-net stations at the same depth (Figure 3c) and recording acceleration. Foregoing research consider a peak acceleration as a measure of damaging due to strong ground motion [e.g., *Schaff and Beroza*, 2004]. *Beresnev and Wen* [1996] pointed out that a peak acceleration is a frequency-dependent measure of maximum

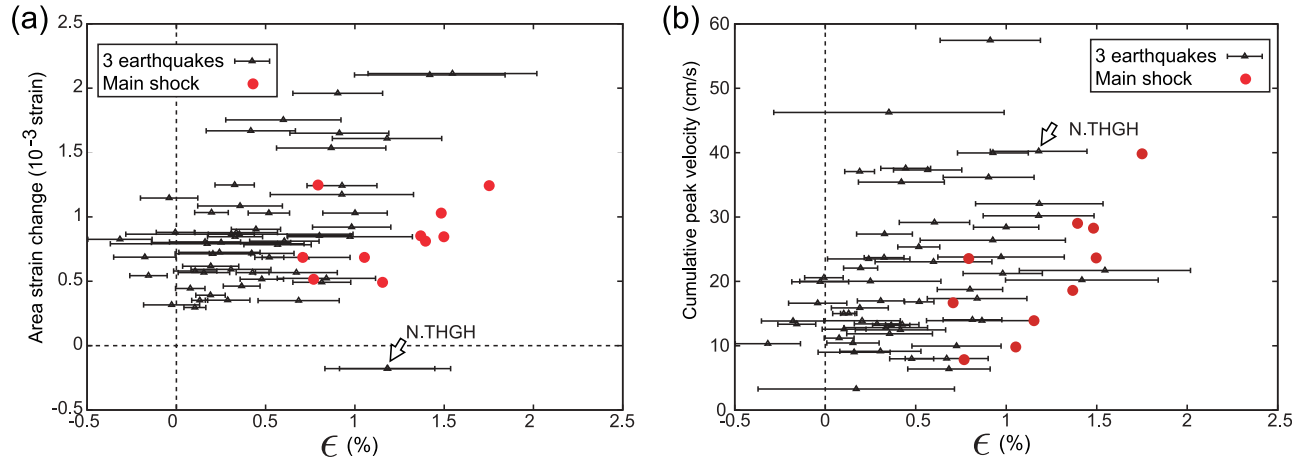


**Figure 4.** (a) Averaged velocity change ($\epsilon$, with standard deviations calculated from preseismic and postseismic values) plotted against area strain change including three earthquakes. (b) Averaged velocity change plotted against cumulative peak particle velocity recorded in three earthquakes. Red dots are data points for the Tohoku-oki earthquake. Arrows show station N.THGH.

strain assuming the sinusoidal displacement input of a one-dimensional transverse wave propagating to $z$-direction ($u = u_0 \sin(\omega t - kz)$) as,

$$\max|\gamma| = \max\left|\frac{\partial u}{\partial z}\right| = \frac{a_0}{\omega V} = \frac{v_0}{V}, \tag{4}$$

where $\gamma$ is a strain, $a_0$ is a peak acceleration, $v_0$ is a peak particle velocity, and $V$ is a propagating velocity [*Beresnev and Wen*, 1996]. In order to obtain frequency-independent measure of maximum strain as a relative damaging, we estimate a peak particle velocity (equation (4)). We obtained the distribution of peak particle velocity from Kik-net data after bandpass filtering from 0.1 to 10 Hz. The cumulative values of peak particle velocity recorded during the three earthquakes (Figure 3c) show a trend similar to those of the velocity change (Figure 3a) and the area strain change (Figure 3b), with the largest particle velocities distributed near the coastline.

[18] Figure 4a shows the average velocity change against the estimated area strain change for each of the Hi-net stations. Similarly, Figure 4b plots the velocity change against the observed cumulative peak particle velocities for the Kik-net stations. Because velocity healing is nonlinear, some stations showed unstable values of $\epsilon$ shortly after earthquakes, and the crossplot of Figure 4b shows much scatter. To reduce scatter, we plotted only the stations that showed clear and stable velocity decreases from the Tohoku-oki earthquake (red dots in Figure 4). Both Figures 4a and 4b show a clear positive correlation of the velocity decrease (positive $\epsilon$). The anomalous station N.THGH showed a velocity decrease even though the area experienced compression (arrow in Figure 4a). The compression was the result of fault activity associated with the two aftershocks (Figure 3b). However, station N.THGH did not experience anomalous particle velocities (arrow in Figure 4b).

[19] This observation suggests that the velocity change estimated in this study is affected by the near-surface strong motion and may correspond to damage to near-surface rocks around 200 m depth. However, the velocity change we measured is smaller than that reported by *Nakata and Snieder* [2011], who estimated a shear velocity decrease of ~5% at a depth of a few hundred meters by cross-correlating earthquakes observed by the Kik-net vertical array. Furthermore, we showed that later arriving events show a smaller velocity change (Figure 2e) and that strain change correlated with velocity change (Figure 4a). The fact that our results are based on scattered waves with traveltimes of 2 to 10 s indicates that the scattered waves are generated at a maximum 25 km depth, considering an average P-wave velocity of 5000 m/s. These results, therefore, support our contention that the velocity change we measured contains information on the results of stress release deep underground in addition to shallow effects due to strong ground motion.

[20] **Acknowledgments.** We thank the National Research Institute for Earth Science and Disaster Prevention for providing the Hi-net and Kik-net data used in this study. We obtained GPS GEONET F3 coordinate data from GSI. S. Minato acknowledges support from a Grant-in-Aid (212666) from the Japan Society for the Promotion of Science Fellows. This study was supported by the Global Center for Education and Research on Human Security for Asian Megacities (GCOE). The useful comments of two anonymous reviewers helped to further improve this article.

[21] The Editor thanks Ulrich Wegler and Roel Snieder for assisting with the evaluation of this paper.

## References

Bensen, G. D., M. H. Ritzwoller, M. P. Barmin, A. L. Levshin, F. Lin, M. P. Moschetti, N. M. Shapiro, and Y. Yang (2007), Processing seismic ambient noise data to obtain reliable broad-band surface wave dispersion measurements, *Geophys. J. Int.*, *169*(3), 1239–1260, doi:10.1111/j.1365-246X.2007.03374.x.

Beresnev, I., and K. Wen (1996), Nonlinear soil response-a reality?, *Bull. Seismol. Soc. Am.*, *86*(6), 1964–1978.

Brenguier, F., M. Campillo, C. Hadziioannou, N. M. Shapiro, R. M. Nadeau, and E. Larose (2008), Postseismic relaxation along the San Andreas fault at Parkfield from continuous seismological observations, *Science*, *321*(5895), 1478–1481, doi:10.1126/science.1160943.

Christensen, N. I., and H. F. Wang (1985), The influence of pore pressure and confining pressure on dynamic elastic properties of Berea Sandstone, *Geophysics*, *50*(2), 207–213, doi:10.1190/1.1441910.

Derode, A., E. Larose, M. Campillo, and M. Fink (2003), How to estimate the Green's function of a heterogeneous medium between two passive sensors? Application to acoustic waves, *Appl. Phys. Lett.*, *83*(15), 3054–3056, doi:10.1063/1.1617373.

Draganov, D., X. Campman, J. Thorbecke, A. Verdel, and K. Wapenaar (2009), Reflection images from ambient seismic noise, *Geophysics*, *74*(5), A63–A67.

Hadziioannou, C., E. Larose, O. Coutant, P. Roux, and M. Campillo (2009), Stability of monitoring weak changes in multiply scattering media with ambient noise correlation: Laboratory experiments, *J. Acoust. Soc. Am.*, *125*(6), 3688–3695, doi:10.1121/1.3125345.

Johnson, P., and A. Sutin (2005), Slow dynamics and anomalous nonlinear fast dynamics in diverse solids, *J. Acoust. Soc. Am.*, *117*(1), 124–130, doi:10.1121/1.1823351.

Larose, E., L. Margerin, A. Derode, B. van Tiggelen, M. Campillo, N. Shapiro, A. Paul, L. Stehly, and M. Tanter (2006), Correlation of random wavefields: An interdisciplinary review, *Geophysics*, *71*(4), SI11–SI21.

Lyakhovsky, V., Y. Ben-Zion, and A. Agnon (1997), Distributed damage, faulting, and friction, *J. Geophys. Res.*, *102*, 27,635–27,649.

Meier, U., N. Shapiro, and F. Brenguier (2010), Detecting seasonal variations in seismic velocities within Los Angeles Basin from correlations of ambient seismic noise, *Geophys. J. Int.*, *181*, 985–996.

Nakata, N., and R. Snieder (2011), Near-surface weakening in Japan after the 2011 Tohoku-Oki earthquake, *Geophys. Res. Lett.*, *38*, L17302, doi:10.1029/2011GL048800.

Nishimura, T., N. Uchida, H. Sato, M. Ohtake, S. Tanaka, and H. Hamaguchi (2000), Temporal changes of the crustal structure associated with the M6.1 earthquake on September 3, 1998, and the volcanic activity of Mount Iwate, Japan, *Geophys. Res. Lett.*, *27*(2), 269–272.

Nishimura, T., H. Munekane, and H. Yarai (2011), The 2011 off the Pacific coast of Tohoku earthquake and its aftershocks observed by GEONET, *Earth Planets Space*, *63*(7), 631–636.

Niu, F., P. Silver, T. Daley, X. Cheng, and E. Majer (2008), Preseismic velocity changes observed from active source monitoring at the Parkfield SAFOD drill site, *Nature*, *454*(7201), 204–208.

Ohmi, S., K. Hirahara, H. Wada, and K. Ito (2008), Temporal variations of crustal structure in the source region of the 2007 Noto Hanto earthquake, central Japan, with passive image interferometry, *Earth Planets Space*, *60*, 1069–1074.

Ozawa, S., T. Nishimura, T. Suito, H. Kobayashi, M. Tobita, and T. Imakiire (2011), Coseismic and postseismic slip of the 2011 magnitude-9 Tohoku-oki earthquake, *Nature*, *475*(7356), 373–377.

Peng, Z., and Y. Ben-Zion (2006), Temporal changes of shallow seismic velocity around the Karadere-Düzce branch of the North Anatolian fault and strong ground motion, *Pure Appl. Geophys.*, *163*, 567–600.

Poupinet, G., W. L. Ellsworth, and J. Frechet (1984), Monitoring velocity variations in the crust using earthquake doublets: An application to the Calaveras Fault, California, *J. Geophys. Res.*, *89*(B7), 5719–5731.

Roux, P., K. G. Sabra, W. A. Kuperman, and A. Roux (2005), Ambient noise cross correlation in free space: Theoretical approach, *J. Acoust. Soc. Am.*, *117*(1), 79–84, doi:10.1121/1.1830673.

Rubinstein, J. L., and G. C. Beroza (2004), Nonlinear strong ground motion in the $M_L$ 5.4 Chittenden earthquake: Evidence that preexisting damage increases susceptibility to further damage, *Geophys. Res. Lett.*, *31*, L23614, doi:10.1029/2004GL021357.

Sawazaki, K., H. Sato, H. Nakahara, and T. Nishimura (2009), Time-lapse changes of seismic velocity in the shallow ground caused by strong ground motion shock of the 2000 Western-Tottori earthquake, Japan, as revealed from coda deconvolution analysis, *Bull. Seismol. Soc. Am.*, *99*(1), 352.

Schaff, D. P., and G. C. Beroza (2004), Coseismic and postseismic velocity changes measured by repeating earthquakes, *J. Geophys. Res.*, *109*, B10302, doi:10.1029/2004JB003011.

Sens-Schönfelder, C., and U. Wegler (2006), Passive image interferometry and seasonal variations of seismic velocities at Merapi Volcano, Indonesia, *Geophys. Res. Lett.*, *33*, L21302, doi:10.1029/2006GL027797.

Shapiro, N. M., M. Campillo, L. Stehly, and M. H. Ritzwoller (2005), High-resolution surface-wave tomography from ambient seismic noise, *Science*, *307*(5715), 1615–1618, doi:10.1126/science.1108339.

Takahashi, H. (2011), Static strain and stress changes in eastern Japan due to the 2011 off the pacific coast of tohoku earthquake, as derived from GPS data, *Earth Planets Space*, *63*(7), 741–744.

TenCate, J. A., E. Smith, and R. A. Guyer (2000), Universal slow dynamics in granular solids, *Phys. Rev. Lett.*, *85*, 1020–1023, doi:10.1103/PhysRevLett.85.1020.

Terada, A., and N. Miyabe (1929), Deformation of the earth crust in Kwansai district and its relation to orographic features, *Bull. Earthquake Res. Inst. Univ. Tokyo*, *7*, 233–239.

Toksöz, M. N., C. H. Cheng, and A. Timur (1976), Velocities of seismic waves in porous rocks, *Geophysics*, *41*(4), 621–645, doi:10.1190/1.1440639.

Tsuji, T., H. Tokuyama, P. Costa Pisani, and G. Moore (2008), Effective stress and pore pressure in the Nankai accretionary prism off the Muroto Peninsula, southwestern Japan, *J. Geophys. Res.*, *113*, B11401, doi:10.1029/2007JB005002.

Vidale, J., and Y. Li (2003), Damage to the shallow Landers fault from the nearby Hector Mine earthquake, *Nature*, *421*(6922), 524–526.

Wapenaar, K., and J. Fokkema (2006), Green's function representations for seismic interferometry, *Geophysics*, *71*(4), SI33–SI46, doi:10.1190/1.2213955.

Weaver, R. L., and O. I. Lobkis (2004), Diffuse fields in open systems and the emergence of the Green's function (l), *J. Acoust. Soc. Am.*, *116*(5), 2731–2734, doi:10.1121/1.1810232.

Wegler, U., and C. Sens-Schönfelder (2007), Fault zone monitoring with passive image interferometry, *Geophys. J. Int.*, *168*(3), 1029–1033, doi:10.1111/j.1365-246X.2006.03284.x.

Wegler, U., H. Nakahara, C. Sens-Schönfelder, M. Korn, and K. Shiomi (2009), Sudden drop of seismic velocity after the 2004 $M_w$ 6.6 mid-Niigata earthquake, Japan, observed with Passive Image Interferometry, *J. Geophys. Res.*, *114*,B06305, doi:10.1029/2008JB005869.

Yoshida, K., A. Hasegawa, T. Okada, T. Iinuma, Y. Ito, and Y. Asano (2012), Stress before and after the 2011 great Tohoku-oki earthquake and induced earthquakes in inland areas of eastern Japan, *Geophys. Res. Lett.*, *39*, L03302, doi:10.1029/2011GL049729.